Sequences Detection of an Unbalanced Sinusoidal Voltage of Unknown Frequency Using a Reduced-Order Observer

Sebastian Gomez Jorge, Jorge A. Solsona, *Senior Member, IEEE*, and Claudio A. Busada

***Abstract*—This paper presents a globally convergent nonlinear observer capable of recovering the positive and negative sequences of an unbalanced grid voltage. The proposed algorithm has frequency adaptation, and is therefore, in steady state, immune to grid frequency variations. Another feature is that since it is a reduced-order observer, only three states are needed to implement it. The validity of the proposed scheme is verified through mathematical analysis, simulation, and experimental results.**

***Index Terms*—Adaptive observer, frequency estimation, reduced-order observer, sequences detection.**

I. Introduction

THE development of power-electronics technologies allows to create distributed-generation systems for powers increasingly higher. This is also creating a trend toward the use of flexible alternating current transmission systems (FACTS) in power systems. Many control strategies have been proposed for these systems, and a problem that arises recurrently is the poor performance under grid voltage unbalanced conditions [1]–[4]. Due to different fault conditions, these unbalances are relatively frequent in distribution networks [5]. This results in most control schemes requiring a fast and precise sequences detection method in order to achieve high-quality energy generation [6]–[8]. Sequence detection can be thought as a subset of the synchronization problem, which is closely related to the estimation of the fundamental frequency. This problem has been extensively studied, and there are numerous topologies to solve it based on phase-locked loop (PLL) [9]–[11] and frequency-locked loop (FLL) [12]–[14]. Sequence detection schemes based on the moving average filters (MAFs) have been proposed in [15] and [16]. These are capable of positive-sequence detection and have frequency adaptation. However, because they are based on MAFs, they require several states to log the sampled data, increasing the memory requirements of their implementation. There are other methods that take advantage of the system's symmetry to reduce the number of states [17], [18], which allows estimating the positive- and negative-sequence components independently, without the need to estimate both. Aiming only for sequences detection, in [19] is a fixed-reference-frame phase-locked loop (FRF-PLL). It is capable of detecting the positive- and negative-sequence components of an unbalanced grid voltage as well as its frequency. Also, a sequence detection scheme based on the extended Kalman filter (EKF) has been presented in [20]. Although this scheme is capable of recovering the positive and negative sequences as well as the frequency of the grid voltage, it requires the online computation of several trigonometric functions, which increase the memory requirements, and it is not supported by any experimental data.

For commercial applications, where cost reduction is important, it is desirable to obtain reduced computational cost algorithms, an objective pursued by many researchers. Therefore, in this paper, a low computational cost algorithm will be proposed. This algorithm is based on a reduced-order observer, and allows to obtain the positive- and negative-sequence components of the grid voltage as well as its frequency. This is achieved using only three states. It will also be shown that for unbalanced grid voltages, the proposed observer is globally convergent.

This paper is organized as follows. In Section II, a description of the system under study is given. In Section III, the proposed observer is presented, analyzed, and a method for tuning its parameters is given. Section V shows simulation and experimental results that validate the proposal. For the sake completeness, Section VI shows a performance comparison of the proposed observer and the FRF-PLL, both for unbalanced and harmonic contaminated voltages. Finally, in Section VII, conclusions are drawn.

II. System Description

Consider that the grid voltage is composed of a sinusoidal signal of positive sequence and one of negative sequence. Also, these signals have the same angular frequency ω, which we will assume slow varying, and are both of constant magnitude. Under these conditions, the grid voltage can be described in an $\alpha\beta$ stationary reference frame as

$$Y_\alpha = V_\alpha^+ + V_\alpha^- \tag{1}$$

$$Y_\beta = V_\beta^+ + V_\beta^- \tag{2}$$

$$V_\alpha^+ = A^+ \cos(\omega t + \phi^+) \tag{3}$$

$$V_\beta^+ = A^+ \sin(\omega t + \phi^+) \tag{4}$$

$$V_\alpha^- = A^- \sin(\omega t + \phi^-) \tag{5}$$

Manuscript received June 08, 2012; revised November 13, 2012; accepted March 15, 2013. Paper no. TPWRD-00586-2012.

The authors are with the Instituto de Investigaciones en Ingeniería Eléctrica (IIIE) "Alfredo Desages" (UNS-CONICET), Departamento de Ingeniería Eléctrica y de Computadoras, Universidad Nacional del Sur (UNS), 8000 Bahía Blanca, Argentina (e-mail: sebastian.gomezjorge@uns.edu.ar; cbusada@uns.edu.ar; jsolsona@uns.edu.ar).

This work was supported by Universidad Nacional del Sur, CONICET and ANPCyT, Argentina.

Digital Object Identifier 10.1109/TPWRD.2013.2253498

$$V_\beta^- = A^- \cos(\omega t + \phi^-) \tag{6}$$

where Y_α and Y_β are the α and β components of the measured grid voltage, V_α^+ and V_β^+ are the $\alpha\beta$ components of the positive-sequence voltage, V_α^- and V_β^- are the $\alpha\beta$ components of the negative-sequence voltage, A^+ and A^- are the positive- and negative-sequence amplitudes, and, finally, ϕ^+ and ϕ^- are their phases, respectively.

Equation (3)–(6) can be described by the following set of differential equations:

$$\dot{V}_\alpha^+ = -\omega V_\beta^+ \tag{7}$$
$$\dot{V}_\beta^+ = \omega V_\alpha^+ \tag{8}$$
$$\dot{V}_\alpha^- = \omega V_\beta^- \tag{9}$$
$$\dot{V}_\beta^- = -\omega V_\alpha^-. \tag{10}$$

Then, defining the new set of states

$$z_1 = Y_\alpha = V_\alpha^+ + V_\alpha^- \tag{11}$$
$$z_2 = -\omega(V_\beta^+ - V_\beta^-) \tag{12}$$
$$z_3 = Y_\beta = V_\beta^+ + V_\beta^- \tag{13}$$
$$z_4 = \omega(V_\alpha^+ - V_\alpha^-) \tag{14}$$

where z_1 and z_3 are equivalent to (1) and (2), respectively, and z_2 and z_4 are their derivatives, the system can be described by the following set of differential equations:

$$\dot{z}_1 = z_2 \tag{15}$$
$$\dot{z}_2 = -\theta z_1 \tag{16}$$
$$\dot{z}_3 = z_4 \tag{17}$$
$$\dot{z}_4 = -\theta z_3 \tag{18}$$

where $\theta = \omega^2$. It is easy to see from (11)–(14) that the sequence components can be recovered from the following set of algebraic equations:

$$V_\alpha^+ = \frac{1}{2}(z_1 + \frac{z_4}{\omega}) \tag{19}$$
$$V_\alpha^- = \frac{1}{2}(z_1 - \frac{z_4}{\omega}) \tag{20}$$
$$V_\beta^+ = \frac{1}{2}(z_3 - \frac{z_2}{\omega}) \tag{21}$$
$$V_\beta^- = \frac{1}{2}(z_3 + \frac{z_2}{\omega}). \tag{22}$$

With these preliminary definitions, we will now proceed to develop our proposal.

III. Proposed Observer

The objective of the proposed observer will be to recover estimates of (19)–(22) from the measured signals (1)–(2) using a minimum number of states.

To begin the development of the observer, lets assume that the signals z_2 and z_4 are available measured signals. This assumption will be dropped later. Then, a typical Luenberger observer to estimate these signals is

$$\dot{\hat{z}}_2 = -\hat{\theta} z_1 + g(z_2 - \hat{z}_2) \tag{23}$$
$$\dot{\hat{z}}_4 = -\hat{\theta} z_3 + g(z_4 - \hat{z}_4) \tag{24}$$

$$\dot{\hat{\theta}} = \mathrm{AL} \tag{25}$$

where $g \in \mathbb{R}$, $g > 0$ is a design constant, $\hat{\theta}$, $\hat{z}_2$, and $\hat{z}_4$ are the estimated signals and AL is an adaptation law to be determined. This adaptation law is chosen through the Lyapunov method such as the convergence to zero of the estimation error is guaranteed. The details of this development are shown in Appendix A, where it is shown that an adaptation law that fulfills these requirements is

$$\dot{\hat{\theta}} = -\gamma\left[z_1(z_2 - \hat{z}_2) + z_3(z_4 - \hat{z}_4)\right] \tag{26}$$

with $\gamma \in \mathbb{R}$, $\gamma > 0$ is a design constant. Now, dropping the assumption that z_2 and z_4 were measured, it is possible to replace them from (15) and (17) to obtain

$$\dot{\hat{z}}_2 = -\hat{\theta} z_1 + g(\dot{z}_1 - \hat{z}_2) \tag{27}$$
$$\dot{\hat{z}}_4 = -\hat{\theta} z_3 + g(\dot{z}_3 - \hat{z}_4) \tag{28}$$
$$\dot{\hat{\theta}} = -\gamma\left[z_1(\dot{z}_1 - \hat{z}_2) + z_3(\dot{z}_3 - \hat{z}_4)\right]. \tag{29}$$

In order to avoid performing the derivatives of the measured signals, the following auxiliary signals are defined:

$$\dot{v}_2 = \dot{\hat{z}}_2 - g\dot{z}_1 = -\hat{\theta} z_1 - g\hat{z}_2 \tag{30}$$
$$\dot{v}_4 = \dot{\hat{z}}_4 - g\dot{z}_3 = -\hat{\theta} z_3 - g\hat{z}_4 \tag{31}$$
$$\dot{v}_\theta = \dot{\hat{\theta}} + \gamma(z_1\dot{z}_1 + z_3\dot{z}_3) = \gamma(z_1\hat{z}_2 + z_3\hat{z}_4) \tag{32}$$

which are obtained by subtracting the newly replaced derivative terms on both sides of (27)–(29). Now, integrating and rearranging these equations results

$$\hat{z}_2 = v_2 + g z_1 \tag{33}$$
$$\hat{z}_4 = v_4 + g z_3, \tag{34}$$
$$\hat{\theta} = v_\theta - \frac{\gamma}{2}(z_1^2 + z_3^2). \tag{35}$$

Replacing these equations in (30)–(32), then replacing the resulting estimated signals in (19)–(22), and recalling (11) and (13), the complete estimation algorithm results

$$\dot{v}_2 = -\left[v_\theta - \frac{\gamma}{2}(Y_\alpha^2 + Y_\beta^2) + g^2\right] Y_\alpha - g v_2 \tag{36}$$
$$\dot{v}_4 = -\left[v_\theta - \frac{\gamma}{2}(Y_\alpha^2 + Y_\beta^2) + g^2\right] Y_\beta - g v_4 \tag{37}$$
$$\dot{v}_\theta = \gamma\left[Y_\alpha v_2 + Y_\beta v_4 + g(Y_\alpha^2 + Y_\beta^2)\right] \tag{38}$$
$$\hat{\omega} = \sqrt{|v_\theta - \frac{\gamma}{2}(Y_\alpha^2 + Y_\beta^2)|} \tag{39}$$
$$\hat{V}_\alpha^+ = \frac{1}{2}(Y_\alpha + \frac{v_4 + gY_\beta}{\hat{\omega}}) \tag{40}$$
$$\hat{V}_\alpha^- = \frac{1}{2}(Y_\alpha - \frac{v_4 + gY_\beta}{\hat{\omega}}) \tag{41}$$
$$\hat{V}_\beta^+ = \frac{1}{2}(Y_\beta - \frac{v_2 + gY_\alpha}{\hat{\omega}}) \tag{42}$$
$$\hat{V}_\beta^- = \frac{1}{2}(Y_\beta + \frac{v_2 + gY_\alpha}{\hat{\omega}}). \tag{43}$$

Note that this reduced-order observer requires the use of only three states and a few algebraic operations to be implemented. Note also that the transformations performed to (23), (24), and (26) do not modify the convergence of the proposal, since they do not add additional dynamics.

IV. Criterion for Tuning the Observer Gains

In Appendix A it is shown that the estimated variables converge to the actual ones asymptotically. The actual convergence speed of these variables depends on the parameters g and γ. In this section a criterion for choosing them in order to achieve a desired dynamic response is given. To this end, we will analyze the dynamic behavior of the proposed algorithm under the assumption of small signal. This analysis will show the relationship between g, γ and the convergence speed of the observer. Since the system is highly nonlinear, as a rough approximation, we will find separate expressions for the convergence time of the estimated sequence components (40)–(43) and the convergence time of the estimated frequency (39).

A. Estimated Sequence Components Convergence Time

Let us assume that the estimated frequency is fixed at the grid's nominal frequency ω_o. This is equivalent to say that the dynamics of states v_2, v_4, and v_θ are decoupled. This assumption does not always hold, but it gives a good starting point for choosing parameter g and then fine tuning it through iteration.

Subtracting (23) and (24) from (16) and (18), respectively, and writing the results in a state variable form, results in

$$\dot{\vec{e}} = \underbrace{\begin{bmatrix} -g & 0 \\ 0 & -g \end{bmatrix}}_{A} \vec{e} \tag{44}$$

where $\vec{e} = [(z_2 - \hat{z}_2)\ (z_4 - \hat{z}_4)]^T$, and we have assumed $\hat{\theta} = \theta$. Since the convergence time of $\vec{e}$ is determined by the eigenvalues of matrix A, it is easy to see that the setting time of these error states to 2% of their final value is given by

$$t_{\text{set}} \simeq \frac{4}{g} \tag{45}$$

and since the estimated sequence components are a linear combination (assuming$\hat{\theta}$ = constant) of the input signal and the estimated states, their convergence time is also determined by (45).

B. Estimated Frequency Convergence Time

Assuming that the frequency of the input signal is initially fixed at its nominal value ω_o, and at some arbitrary time instant is allowed a small step variation $\triangle\omega$, a linear model that describes the dynamic behavior of the frequency estimator (39) is developed in Appendix B. As described there, the transfer function that relates a grid frequency variation $\triangle\omega$ with an estimated frequency variation $\triangle\hat{\omega}$ is given by

$$\triangle\hat{\omega} = \frac{\gamma K}{2} \frac{(s+2g)\triangle\omega}{s^3 + 2gs^2 + (g^2 + \omega_o^2 + \gamma K)s + \gamma g K} \tag{46}$$

where $K = (A^+)^2 + (A^-)^2$.Fig. 1 shows the root locus of (46) for $A^+ = 311$ V, $A^- = 31$ V, different values of g and different values of γ. The root locus for $g = 100$ is shown with dots, for $g = 200$ with circles and for $g = 300$ with triangles. In the figure, there are also arrows indicating the direction in which the poles move as γ increases. The locus is shown for $0.1 \leq \gamma \leq 1$. According to (45), choosing $g = 300$ the estimated sequence components can achieve a setting time of 13 ms. For this value of g and $\gamma = 0.8$ the poles of the transfer function are at $p_1 = -110$ and $p_{23} - 245 \pm j391$, as shown in Fig. 1. Taking the real pole as the dominant one, the setting time of the estimated frequency to 2% of its final value can be approximated as

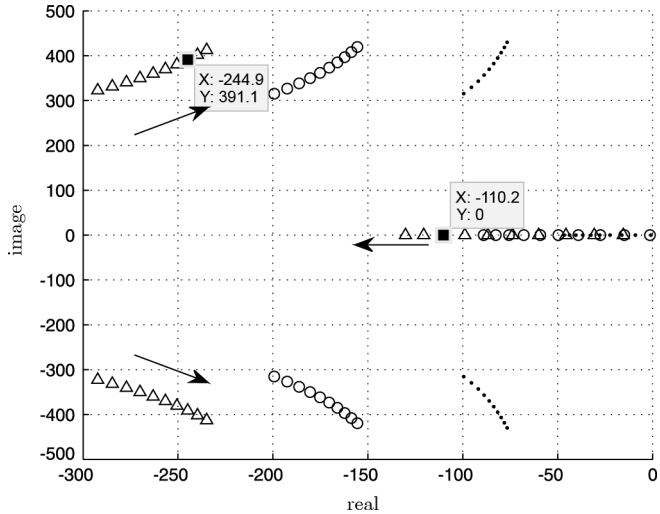

Fig. 1. Root locus of (46) for $A^+ = 311$ V, $A^- = 31$ V, $\omega_o = 2\pi 50$ rad/s, $g = 100$ (dot), $g = 200$ (circle), $g = 300$ (triangle), and $0.1 \leq \gamma \leq 1$.

$$t_{\hat{\omega} set} \simeq \frac{4}{p_1} \simeq 36.36 \text{ ms}. \tag{47}$$

Fig. 2 shows the response of the linearized frequency estimator (46) (dashed line) to an input signal frequency step change (dash/dot line) along with the response of the actual frequency estimator (39) (solid line), all normalized with respect to $\omega_o = 2\pi 50$ rad/s. The parameters for this simulation where $A^+ = 311$ V, $A^- = 31$ V, $g = 300$ and $\gamma = 0.8$. As the figure shows, (46) gives a good approximation of the actual frequency estimator response to an input frequency step change, and converges to 2% of its final value within approximately 35 ms, as was predicted by (47).

V. Simulation and Experimental Results

In this section, we will show simulation and experimental results to validate the proposal. For the simulation and experimental results, the grid voltage is initially composed of a pure sinusoidal signal of magnitude $A^+ = 311$ V and frequency $\omega_o = 2\pi 50$. At time $t = 40$ ms, the grid voltage has a -10% magnitude variation. Then, at $t = 80ms$, this magnitude is reestablished to $A^+ = 311$ V. At that same time instant, the grid is unbalanced with a negative-sequence voltage of magnitude $A^- = 31$ V. Finally, at time $t = 140$ ms, the grid voltage has a frequency step variation of $-2\%\omega_o$. The observer parameters for the simulation and experimental results where $g = 300$ and $\gamma = 0.8$.

A. Simulations

Fig. 3 shows the simulation results. Fig. 3(a) and (b) shows the estimated positive-sequence α and β components of the grid voltage, respectively, with solid line. Also, in those figures, the error between the actual and estimated voltages is shown with dashed line, scaled by a factor of 10 in order to be visible. As these figures show, the magnitude variations at $t = 40$ ms and

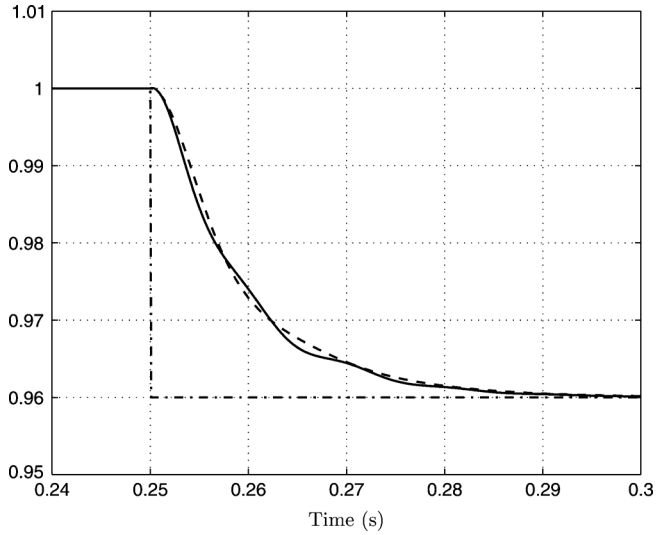

Fig. 2. Linearized frequency estimator simulation normalized with respect to $\omega_o = 2\pi 50\ \mathrm{rad/s}$. Actual input frequency (dash/dot line), linearized frequency estimator (46) (dashed line), and actual frequency estimator (39) (solid line).

$t = 80$ ms are tracked within less than 20 ms, as expected. It can also be seen that the voltage tracking error during the frequency transient produced at $t = 140$ ms relatively small, and its convergence time depends mainly on the convergence of the estimated frequency.

Fig. 3(c) and (d) shows the estimated negative-sequence α and β components of the grid voltage, respectively, with a solid line. Here, the error between the actual and estimated voltages is also shown with a dashed line. The transient response shown in these figures is very similar that shown in the previous two. It can be seen that the observer is clearly able to detect the negative-sequence component introduced at $t = 80$ ms.

Finally, Fig. 3(e) shows the grid frequency (solid line) along with the estimated frequency (dashed line), both normalized with respect to the nominal grid frequency ω_o. As expected, the grid voltage magnitude variations produce transients on the estimated frequency. This is due to the chosen modeling of the system, which assumes voltages of constant magnitude. Nevertheless, it can be seen that the estimated frequency converges to the actual frequency after the transients. Also, the figure shows that the estimated frequency is able to track the grid frequency variation produced at $t = 140$ ms within 35 ms, as expected.

As these figures show, the observer is able to track both the positive and negative-sequence components of the grid voltage, as well as its frequency.

B. Experimental

Fig. 4 shows the experimental results. These were obtained using a fixed point DSP TMS320F2812 working at a clock frequency of 150 MHz. The discretization of the observer was performed replacing the continuous integrators by discrete trapezoidal integrators, with a sample frequency to $f_s = 10$ kHz. All of the signals shown in the figure were captured through the PWM outputs of the DSP after being filtered with an RC low-pass filter with a cutoff frequency of 2.34 kHz.

Fig. 4(a) and (b) shows the estimated positive-sequence α and β components of the grid voltage, respectively, along with

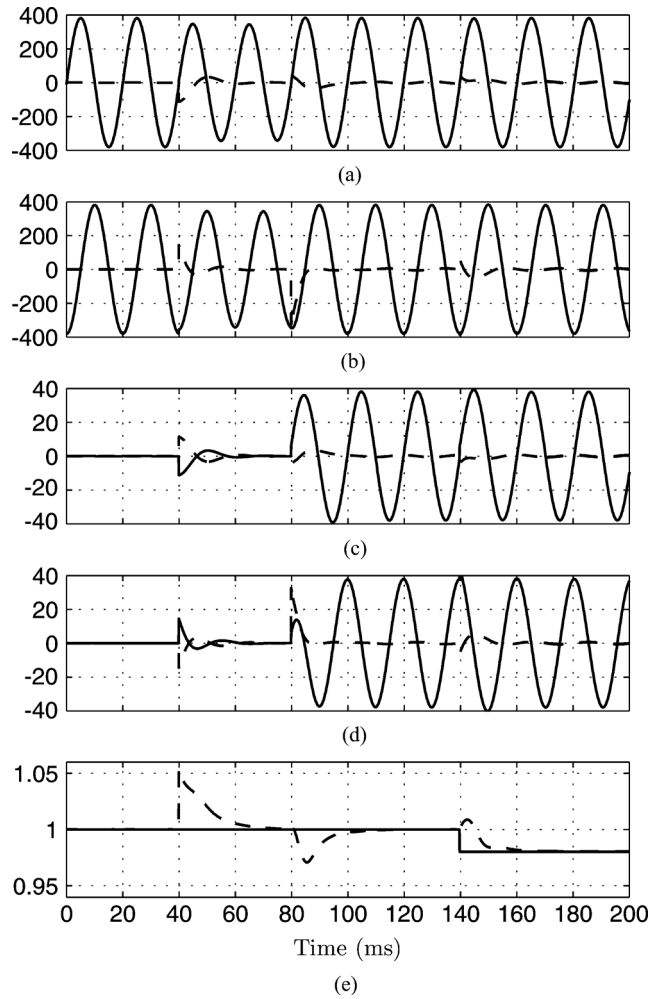

Fig. 3. Simulation results. (a) Estimated positive-sequence α component and estimation error. (b) Estimated positive-sequence β component and estimation error. (c) Estimated negative-sequence α component and estimation error. (d) Estimated negative-sequence β component and estimation error. (e) Actual and estimated frequencies.

the error between the actual and estimated voltages, scaled by a factor of 10 in order to be visible. Fig. 4(c) and (d) shows the estimated negative-sequence α and β components of the grid voltage, respectively, along with the error between the actual and estimated voltages. Finally, Fig. 4(d) shows both the actual and the estimated grid voltage frequencies. As can be seen, the experimental results match the simulation results almost exactly, which proves the validity of the proposed approach.

Regarding the computational burden, the calculation of both sequences and the frequency takes $3.95\ \mu$s , that is, 3.9% of the available computation time for the chosen sampling time, which is clearly a very low burden. As a comparison, it can be mentioned that the MCCF [17] requires $7.6\ \mu$s and the MSOGI-FLL [14] requires $6.74\ \mu$s to estimate the same signals.

VI. Performance and Structure Comparison

In this section the performance of the proposed observer will be compared to the performance of the FRF-PLL proposed in [19]. To do so, both estimators are simulated when in presence of grid voltage variations and their dynamic responses are compared. First for a grid with unbalance, and later for a grid with

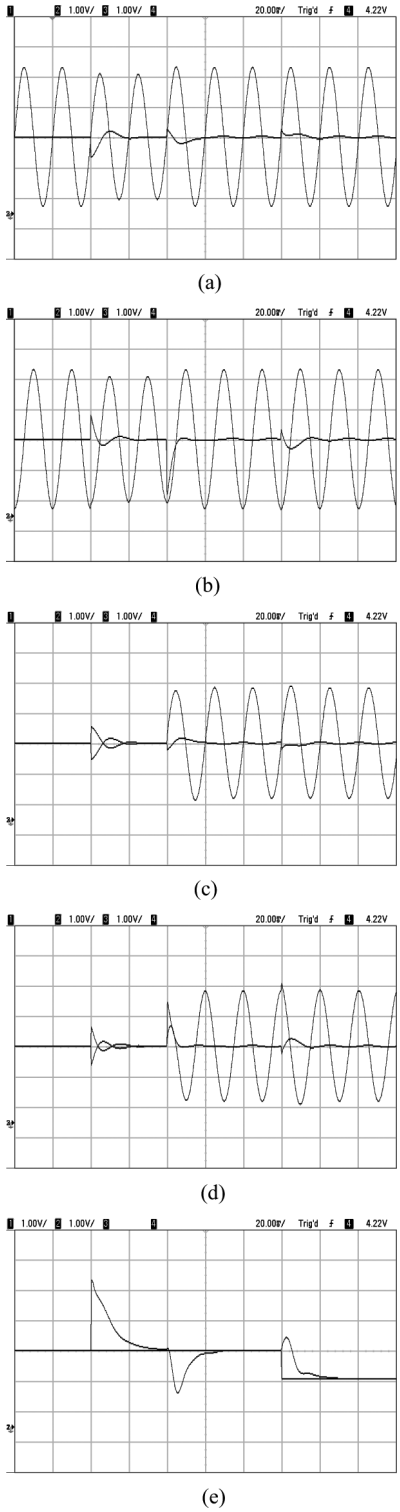

Fig. 4. Experimental results (horizontal scale: 20 ms/div). (a) $\hat{V}_{\alpha}^{+}$ scale: 160 V/div, error scale: 160 V/div. (b) $\hat{V}_{\beta}^{+}$ scale: 160 V/div, error scale: 160 V/div. (c) $\hat{V}_{\alpha}^{-}$ scale: 20 V/div, error scale: 20 V/div. (d) $\hat{V}_{\beta}^{-}$ scale: 20 V/div, error scale: 20 V/div. (e) ω, $\hat{\omega}$ scale: $2\%\omega_o/div$.

unbalance and a fifth harmonic. This also allows to evaluate the performance of the proposal when in presence of non modeled harmonics.

For the first simulation the grid voltage is composed of a positive-sequence signal of magnitude $A^{+} = 311$ V and negative-sequence signal of magnitude $A^{-} = 0.3A^{+}$. For the second one, the grid voltage also has a negative-sequence fifth harmonic signal of magnitude $A^{-5} = 0.05A^{+}$. At time $t = 40$ ms the grid voltage has a -10% magnitude variation. Then, at $t = 80$ ms this magnitude is reestablished to $A^{+} = 311$ V. Finally, at time $t = 140$ ms, the grid voltage has a frequency step variation of $-2\%\omega_o$. The observer parameters of the proposed observer where $g = 300$ and $\gamma = 0.8$, whereas the parameters of the FRF-PLL where $\lambda = 300$ and $\gamma = 0.86$. These values where chosen to obtain the same dynamic response as shown in [19], where γ had to be modified to take into account the difference in the grid voltage magnitude (100 V versus 311 V) and the Park transform constant $(2/3 \text{vs} \sqrt{2/3})$.

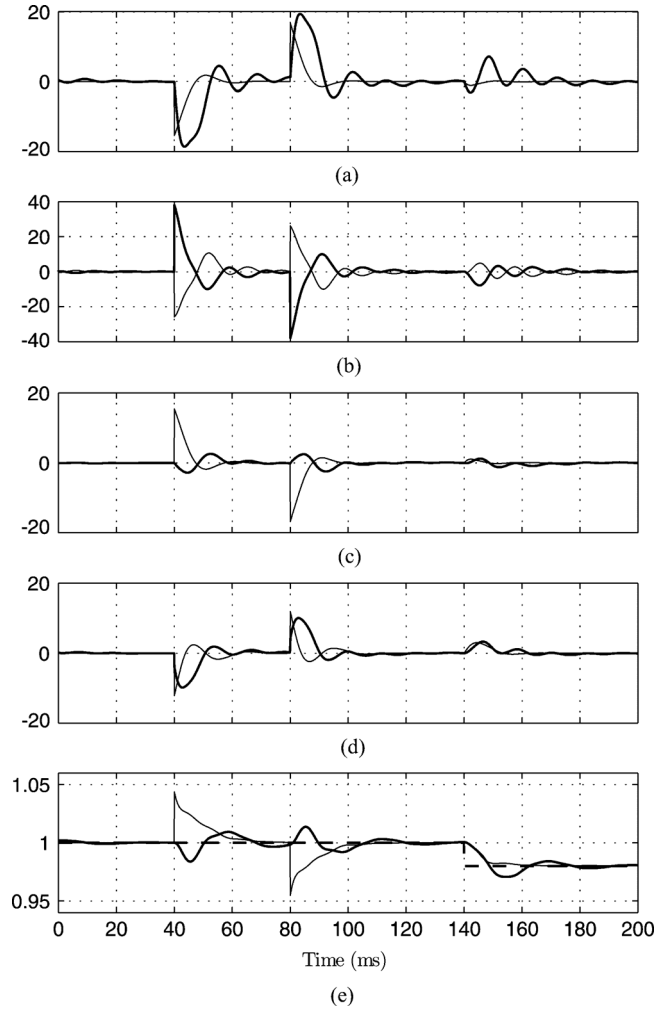

Fig. 5. Performance comparison for the unbalanced grid. (a) FRF-PLL and proposed observer positive-sequence α component tracking error. (b) FRF-PLL and proposed observer positive-sequence β component tracking error. (c) FRF-PLL and proposed observer negative-sequence α component tracking error. (d) FRF-PLL and proposed observer negative-sequence β component tracking error. (e) Actual, FRF-PLL estimated and proposed observer estimated frequencies.

Fig. 5 shows the simulated comparison results for an unbalanced grid voltage. Fig. 5(a) and (b) shows the α and β positive-sequence components tracking error of both estimators. As these figures show, the magnitude variations at $t = 40$ ms and $t = 80$ ms are tracked by the FRF-PLL with a slightly underdamped response. The same happens for the frequency transient

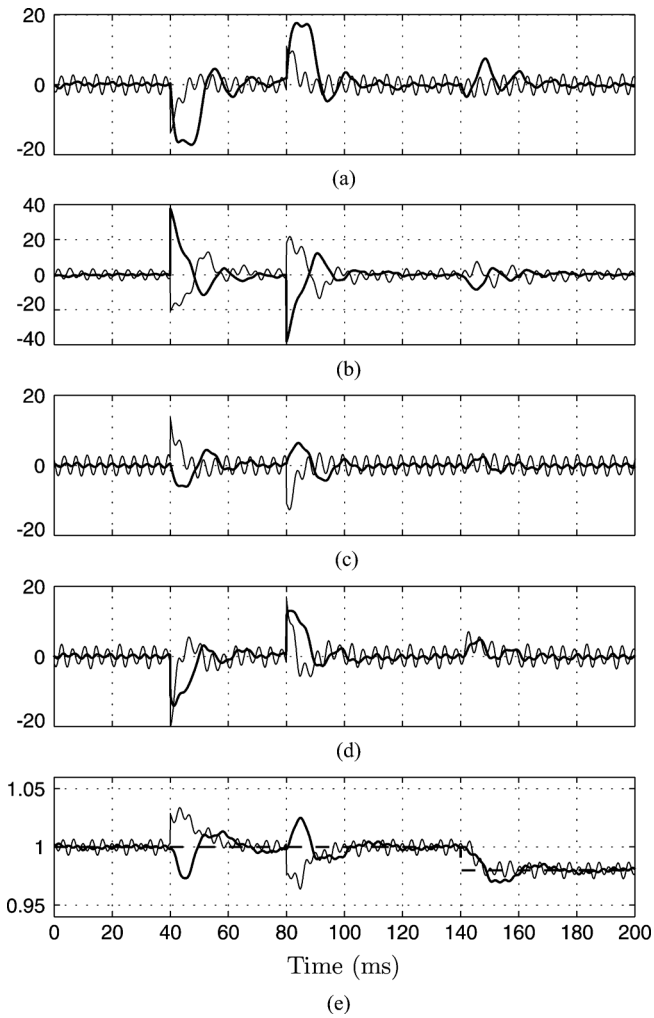

Fig. 6. Performance comparison for unbalanced and 5th harmonic contaminated grid. (a) FRF-PLL and proposed observer positive-sequence α component tracking error. (b) FRF-PLL and proposed observer positive-sequence β component tracking error. (c) FRF-PLL and proposed observer negative-sequence α component tracking error. (d) FRF-PLL and proposed observer negative-sequence β component tracking error. (e) Actual, FRF-PLL estimated and proposed observer estimated frequencies.

produced at $t = 140$ ms. Fig. 5(c) and (d) shows the α and β negative-sequence components tracking error of both estimators. The transient response shown in these figures is very similar that shown in the previous two. Finally, Fig. 5(e) shows the grid frequency (dashed line) along with the FRF-PLL estimated frequency (thick line) and the proposed observer estimated frequency (thin line), all normalized with respect to the nominal grid frequency ω_o. As can be seen, the FRF-PLL frequency estimator has a slightly underdamped response. As these figures show, the dynamic responses of both estimators are similar.

Fig. 6 shows the same results as the previous figure, but in this case the grid voltage is contaminated with a fifth harmonic. As can be seen, the dynamic responses of both estimators behave similarly to the previous case. However, the proposed observer is unable to fully reject the harmonic contamination. In this case, the total harmonic distortions (THDs) of the FRF-PLL positive-sequence α and β components are 0.15% and 0.16%, respectively, whereas for the proposed observer, these are 0.66% and 0.71%. For the negative-sequence components, the FRF-PLL THDs are 0.44% and 0.48% for the α and β components, whereas for the proposed observer, these are 2.43% and 2.45%, respectively. The lower harmonic rejection capability of the proposed observer is to be expected, since one characteristic of the reduced-order observers is that the measured signal is not estimated, and used straight out to obtain the estimated outputs. However, in systems where the distortion is small, such as high-voltage systems, where the main component that arises during a fault scenario is the negative-sequence fundamental component, the performance of both estimators is similar.

Regarding the structure comparison, the proposed scheme requires computing three differential equations and five algebraic equations, whereas the implementation of the FRF-PLL requires computing five differential equations and three algebraic equations. In both algorithms, a square root must be computed in order to obtain the estimated angular frequency.

VII. Conclusions

This paper presents a nonlinear reduced-order observer that allows to estimate the positive and negative sequences of an unbalanced sinusoidal grid voltage. Furthermore, the proposed observer is frequency adaptive, and its implementation allows obtaining a very low computational burden algorithm. Moreover, the global convergence of the observer is proven and a linear approximation of the frequency estimator dynamics, which can be used to tune its parameters, is given. A performance and structure comparison with the FRF-PLL is performed. For signals with low harmonic distortion, the results obtained in this paper show that the performance of both algorithms is similar. However, the proposed method does not offer very good response when the input signal is contaminated with harmonics.

Appendix A

To find the adaptation law, Lyapunov stability theory will be used. Defining the error signals $e_2 = z_2 - \hat{z}_2$, $e_4 = z_4 - \hat{z}_4$, their derivatives can be found by subtracting (23) from (16) and (24) from (18), which result

$$\dot{e}_2 = -e_\theta z_1 - g e_2 \tag{48}$$

$$\dot{e}_4 = -e_\theta z_3 - g e_4 \tag{49}$$

where $e_\theta = \theta - \hat{\theta}$. Defining the positive definite candidate Lyapunov function

$$V = \frac{1}{2}(e_2^2 + e_4^2 + \gamma^{-1} e_\theta^2) \tag{50}$$

its derivative results

$$\dot{V} = e_2 \dot{e}_2 + e_4 \dot{e}_4 + \gamma^{-1} e_\theta \dot{e}_\theta \tag{51}$$

where $\gamma \in \mathbb{R}$, $\gamma > 0$ is a design constant. Replacing (48) and (49) in this equation and operating, we obtain

$$\dot{V} = -g(e_2^2 + e_4^2) - e_\theta(z_1 e_2 + z_3 e_4 - \gamma^{-1} \dot{e}_\theta). \tag{52}$$

Forcing the second term of this last equation equal to zero and noting that since θ is constant, $\dot{\theta} = 0$ so $\dot{e}_\theta = -\dot{\hat{\theta}}$, we have

$$\begin{aligned} 0 &= z_1 e_2 + z_3 e_4 + \gamma^{-1}\dot{\hat{\theta}} \\ \dot{\hat{\theta}} &= -\gamma\left[z_1(z_2 - \hat{z}_2) + z_3(z_4 - \hat{z}_4)\right] \end{aligned} \tag{53}$$

which is the adaptation law AL defined in (26). Consequently, the error dynamics is described by

$$\dot{e}_2 = -e_\theta z_1 - g e_2 \tag{54}$$

$$\dot{e}_4 = -e_\theta z_3 - g e_4 \tag{55}$$

$$\dot{e}_\theta = \gamma\left(z_1 e_2 + z_3 e_4\right). \tag{56}$$

The system (54)–(56) can be written in the following form:

$$\dot{\vec{e}} = A\vec{e} + \Gamma^T(\vec{e}, e_\theta, t) e_\theta \tag{57}$$

$$\dot{e}_\theta = \Lambda\Gamma(\vec{e}, e_\theta, t) P\vec{e} \tag{58}$$

where

$$\vec{e} = \begin{bmatrix} e_2 & e_4 \end{bmatrix}^T; z = e_\theta; \Gamma = \begin{bmatrix} -z_1 & -z_3 \end{bmatrix};$$
$$A = \begin{bmatrix} -g & 0 \\ 0 & -g \end{bmatrix}; \Lambda = \gamma; P = \begin{bmatrix} 1 & 0 \\ 0 & 1 \end{bmatrix}.$$

For this system, the origin $(\vec{e}, e_\theta) = 0$ is a globally uniformly asymptotically stable equilibrium point according to the theorem given in [21], [p · 361] since A is Hurwitz; $\Gamma(\vec{e}, e_\theta, t)$ is a matrix of smooth functions uniformly bounded for every $(\vec{e}, e_\theta)$ bounded; P is the symmetric positive definite solution of the Lyapunov equation $A^T P + PA = -Q$, with Q any symmetric positive definite matrix; Λ is a positive definite matrix; $\partial\Gamma/\partial t$ is uniformly bounded for every $(\vec{e}, e_\theta)$ bounded, since z_1 and z_3 are sums of sinusoidal signals; and the function $\alpha = \rho e_\theta^2$ with $\rho \leq \min(z_1^2 + z_3^2)$ is a class K function satisfying $e_\theta^T \Gamma(0, e_\theta, t)\Gamma^T(0, e_\theta, t) e_\theta \geq \alpha$.

APPENDIX B

In order to find the linearized model, we will split the proposed observer into two fictitious observers: one for the positive sequence and one for the negative sequence of the input signal. These observers estimate phasors, hence, they can be transformed, using a proper Park transform, to a rotating frame in which their variables become constants in steady state. Under these assumptions, we can apply Taylor linearization around the steady-state point to obtain a linear model of the observer.

Defining

$$\hat{z}_1 = \hat{V}_\alpha^+ + \hat{V}_\alpha^-, \tag{59}$$

$$\hat{z}_2 = -\omega(\hat{V}_\beta^+ - \hat{V}_\beta^-) \tag{60}$$

$$\hat{z}_3 = \hat{V}_\beta^+ + \hat{V}_\beta^-, \tag{61}$$

$$\hat{z}_4 = \omega(\hat{V}_\alpha^+ - \hat{V}_\alpha^-) \tag{62}$$

and then, replacing these equations and (7)–(10) in (23) and (24), the resulting equations can be separated into two observers, one for the positive and one for the negative sequences

$$\dot{\hat{V}}_\alpha^+ = -\frac{\hat{\theta}}{\omega} V_\beta^+ + g(V_\alpha^+ - \hat{V}_\alpha^+) - \frac{\dot{\omega}}{\omega}\hat{V}_\alpha^+ \tag{63}$$

$$\dot{\hat{V}}_\beta^+ = \frac{\hat{\theta}}{\omega} V_\alpha^+ + g(V_\beta^+ - \hat{V}_\beta^+) - \frac{\dot{\omega}}{\omega}\hat{V}_\beta^+ \tag{64}$$

$$\dot{\hat{V}}_\alpha^- = \frac{\hat{\theta}}{\omega} V_\beta^- + g(V_\alpha^- - \hat{V}_\alpha^-) - \frac{\dot{\omega}}{\omega}\hat{V}_\alpha^- \tag{65}$$

$$\dot{\hat{V}}_\beta^- = -\frac{\hat{\theta}}{\omega} V_\alpha^- + g(V_\beta^- - \hat{V}_\beta^-) - \frac{\dot{\omega}}{\omega}\hat{V}_\beta^- \tag{66}$$

which represent the positive- and a negative-sequence estimates of the input signal. These equations can be written in a compact form using complex notation as

$$\dot{\hat{V}}_{\alpha\beta}^+ = j\frac{\hat{\theta}}{\omega} V_{\alpha\beta}^+ + g(V_{\alpha\beta}^+ - \hat{V}_{\alpha\beta}^+) - \frac{\dot{\omega}}{\omega}\hat{V}_{\alpha\beta}^+, \tag{67}$$

$$\dot{\hat{V}}_{\alpha\beta}^- = -j\frac{\hat{\theta}}{\omega} V_{\alpha\beta}^- + g(V_{\alpha\beta}^- - \hat{V}_{\alpha\beta}^-) - \frac{\dot{\omega}}{\omega}\hat{V}_{\alpha\beta}^- \tag{68}$$

where $V_{\alpha\beta}^+ = V_\alpha^+ + jV_\beta^+$ and $V_{\alpha\beta}^- = V_\alpha^- + jV_\beta^-$. Using these definitions and the fact that $\dot{\hat{\theta}} = 2\hat{\omega}\dot{\hat{\omega}}$, (53) can be rewritten as

$$\begin{aligned} \dot{\hat{\omega}} = \frac{\gamma\omega}{2\hat{\omega}}(&\hat{V}_{\alpha\beta}^+ \otimes V_{\alpha\beta}^+ + V_{\alpha\beta}^- \otimes \hat{V}_{\alpha\beta}^- \\ &+ 2V_{\alpha\beta}^- \otimes V_{\alpha\beta}^+ + V_{\alpha\beta}^+ \otimes \hat{V}_{\alpha\beta}^- + \hat{V}_{\alpha\beta}^+ \otimes V_{\alpha\beta}^-) \end{aligned} \tag{69}$$

where $\otimes$ stands for cross product. Note that the last three terms in this equation represent the cross product of signals of different sequence, hence, they do not change the mean value of $\hat{\omega}$ and, therefore, will be neglected. To find a linearization of (67)–(69) we will transform them to a rotating frame in which their variables become constants in steady state. For the positive-sequence estimate, that means applying a Park transformation rotating with frequency ω, and for the negative sequence one rotating with frequency $-\omega$. These transforms are

$$P^+ = e^{-j\omega t + \phi^+}, \tag{70}$$

$$P^- = e^{j\omega t + \phi^-}. \tag{71}$$

Transforming (67) using P^+, (68) using P^- and (69) using both, we obtain

$$\dot{\hat{V}}_{dq}^+ = (g + j\frac{\hat{\omega}^2}{\omega})V_{dq}^+ - (g + \frac{\dot{\omega}}{\omega} + j\omega)\hat{V}_{dq}^+ \tag{72}$$

$$\dot{\hat{V}}_{dq}^- = (g - j\frac{\hat{\omega}^2}{\omega})V_{dq}^- - (g + \frac{\dot{\omega}}{\omega} - j\omega)\hat{V}_{dq}^- \tag{73}$$

$$\dot{\hat{\omega}} = \frac{\gamma\omega}{2\hat{\omega}}(\hat{V}_{dq}^+ \otimes V_{dq}^+ + V_{dq}^- \otimes \hat{V}_{dq}^-) \tag{74}$$

where $V_{dq}^+ = P^+ V_{\alpha\beta}^+$, $V_{dq}^- = P^- V_{\alpha\beta}^-$, and the last three terms of (69) have been neglected. Lets now assume that steady state has been reached, and that at time $t = t_o$, the input voltage has a frequency step $\triangle\omega$. Then, using Taylor's approximation, (74) linearization is given by

$$\begin{aligned} \triangle\dot{\hat{\omega}} = &\left.\frac{d\dot{\hat{\omega}}}{d\hat{V}_d^+}\right|_{t_o} \triangle\hat{V}_d^+ + \left.\frac{d\dot{\hat{\omega}}}{d\hat{V}_q^+}\right|_{t_o} \triangle\hat{V}_q^+ \\ &+ \left.\frac{d\dot{\hat{\omega}}}{d\hat{V}_d^-}\right|_{t_o} \triangle\hat{V}_d^- + + \left.\frac{d\dot{\hat{\omega}}}{d\hat{V}_q^-}\right|_{t_o} \triangle\hat{V}_q^- \end{aligned} \tag{75}$$

where $d\dot{\hat{\omega}}/d\hat{V}_d^+\Big|_{t_o} = \gamma/2V_{qo}^+$, $d\dot{\hat{\omega}}/d\hat{V}_q^+\Big|_{t_o} = -\gamma/2V_{do}^+$, $d\dot{\hat{\omega}}/d\hat{V}_d^-\Big|_{t_o} = -\gamma/2V_{qo}^-$, $d\dot{\hat{\omega}}/d\hat{V}_q^-\Big|_{t_o} = \gamma/2V_{do}^-$, with $V_{dqo}^+ = V_{do}^+ + jV_{qo}^+$ and $V_{dqo}^- = V_{do}^- + jV_{qo}^-$, which are the positive- and negative-sequence input steady-state value. From the definitions given in (3)–(6) and the Park transforms (70)–(71), the initial conditions are $V_{dqo}^+ = jA^+$ and $V_{dqo}^- = A^-$. Then

$$\triangle\dot{\hat{\omega}} = \frac{\gamma}{2}(A^+\triangle\hat{V}_d^+ + A^-\triangle\hat{V}_q^-). \tag{76}$$

We will now linearize (72) and (73). Since the input frequency is forced a step variation, then $\dot{\omega} = \triangle\omega\delta(t-t_o)$, where $\delta(t)$ is the Dirac delta. To avoid differentiating this when performing the linearization, define the following auxiliary signals $\dot{x}^+ = \dot{\hat{V}}_{dq}^+ + \dot{\omega}/\omega\hat{V}_{dq}^+$ and $\dot{x}^- = \dot{\hat{V}}_{dq}^- + \dot{\omega}/\omega\hat{V}_{dq}^-$. Then, it is easy to see that

$$x^+ = \hat{V}_{dq}^+ + \frac{V_{dqo}^+}{w_o}\triangle\omega \tag{77}$$

$$x^- = \hat{V}_{dq}^- + \frac{V_{dqo}^-}{w_o}\triangle\omega \tag{78}$$

where ω_o is the input frequency value at time $t = t_o$. Equation (72)–(73) can be rewritten in terms of (77) and (78) as

$$\dot{x}^+ = (g + j\frac{\hat{\omega}^2}{\omega})V_{dq}^+ - (g + j\omega)\hat{V}_{dq}^+ \tag{79}$$

$$\dot{x}^- = (g - j\frac{\hat{\omega}^2}{\omega})V_{dq}^- - (g - j\omega)\hat{V}_{dq}^-. \tag{80}$$

Their small-signal variations can be found, using Taylor's approximation, as

$$\triangle\dot{x}^+ = \left.\frac{d\dot{x}^+}{d\hat{V}_{dq}^+}\right|_{t_o}\triangle\hat{V}_{dq}^+ + \left.\frac{d\dot{x}^+}{d\hat{\omega}}\right|_{t_o}\triangle\hat{\omega} + \left.\frac{d\dot{x}^+}{d\omega}\right|_{t_o}\triangle\omega \tag{81}$$

$$\triangle\dot{x}^- = \left.\frac{d\dot{x}^-}{d\hat{V}_{dq}^-}\right|_{t_o}\triangle\hat{V}_{dq}^- + \left.\frac{d\dot{x}^-}{d\hat{\omega}}\right|_{t_o}\triangle\hat{\omega} + \left.\frac{d\dot{x}^-}{d\omega}\right|_{t_o}\triangle\omega \tag{82}$$

where $d\dot{x}^+/d\hat{V}_{dq}^+\Big|_{t_o} = -g - j\omega_o$, $d\dot{x}^+/d\omega|_{t_o} = -j2V_{dqo}^+$, $d\dot{x}^+/d\hat{\omega}|_{t_o} = j2V_{dqo}^+$, $d\dot{x}^-/d\hat{V}_{dq}^-\Big|_{t_o} = -g + j\omega_o$, $d\dot{x}^-/d\omega|_{t_o} = j2V_{dqo}^-$, $d\dot{x}^-/d\hat{\omega}|_{t_o} = -j2V_{dqo}^-$. Replacing (77) in (81) and (78) in (82), and then applying the Laplace operator s, we can obtain the d component of the linearized variation of the positive-sequence signal and the q component of the negative-sequence one

$$\triangle\hat{V}_d^+ = \frac{A^+[(s+2g)\triangle\omega - 2(s+g)\triangle\hat{\omega}]}{s^2 + 2gs + g^2 + \omega_o^2} \tag{83}$$

$$\triangle\hat{V}_q^- = \frac{A^-[(s+2g)\triangle\omega - 2(s+g)\triangle\hat{\omega}]}{s^2 + 2gs + g^2 + \omega_o^2}. \tag{84}$$

Finally, replacing these equations in (76) and operating, we obtain the linearized model of the closed-loop frequency estimator as a function of the input signal frequency variation

$$\triangle\hat{\omega} = \frac{\gamma K}{2}\frac{(s+2g)\triangle\omega}{s^3 + 2gs^2 + (g^2 + \omega_o^2 + \gamma K)s + \gamma gK} \tag{85}$$

where $K = (A^+)^2 + (A^-)^2$. As can be seen, this equation has a dc gain of 1, and models the dynamic response of the frequency estimator as the dynamic of a third-order linear system.

REFERENCES

[1] B. Blazic and I. Papic, "A new mathematical model and control of d-statcom for operation under unbalanced conditions," *Elect. Power Syst. Res.*, vol. 72, no. 3, pp. 279–287, 2004.

[2] K. Li, J. Liu, Z. Wang, and B. Wei, "Strategies and operating point optimization of statcom control for voltage unbalance mitigation in three—phase three—wire systems," *IEEE Trans. Power Del.*, vol. 22, no. 1, pp. 413–422, Jan. 2007.

[3] Y. Liao, H. Li, J. Yao, and K. Zhuang, "Operation and control of a grid—connected dfig—based wind turbine with series grid-side converter during network unbalance," *Elect. Power Syst. Res.*, vol. 81, no. 1, pp. 228–236, 2011.

[4] A. Ajami and M. Armaghan, "Fixed speed wind farm operation improvement using current-source converter based upqc," *Energy Convers. Manage.*, vol. 58, no. 0, pp. 10–18, 2012.

[5] M. Bollen and L. Zhang, "Different methods for classification of three-phase unbalanced voltage dips due to faults," *Elect. Power Syst. Res.*, vol. 66, no. 1, pp. 59–69, 2003.

[6] R. Gupta, A. Ghosh, and A. Joshi, "Performance comparison of vsc-based shunt and series compensators used for load voltage control in distribution systems," *IEEE Trans. Power Del.*, vol. 26, no. 1, pp. 268–278, Jan. 2011.

[7] Y. Wang and L. Xu, "Coordinated control of dfig and fsig-based wind farms under unbalanced grid conditions," *IEEE Trans. Power Del.*, vol. 25, no. 1, pp. 367–377, Jan. 2010.

[8] M. Kamh and R. Iravani, "Unbalanced model and power-flow analysis of microgrids and active distribution systems," *IEEE Trans. Power Del.*, vol. 25, no. 4, pp. 2851–2858, Oct. 2010.

[9] M. Padua, S. Deckmann, and F. Marafao, "Frequency—adjustable positive sequence detector for power conditioning applications," in *Proc. IEEE 36th Power Electron. Specialists Conf.*, Jun. 2005, pp. 1928–1934.

[10] S. O. Da Silva, R. Novochadlo, and R. Modesto, "Single-phase PLL structure using modified p-q theory for utility connected systems," in *Proc. IEEE Power Electron. Specialists Conf.*, Jun. 2008, pp. 4706–4711.

[11] F. Hassan and R. Critchley, "A robust PLL for grid interactive voltage source converters," in *Proc. 14th Int. Power Electron. Motion Control Conf.*, Sep. 2010, pp. T2-29–T2-35.

[12] P. Rodríguez, A. Luna, M. Ciobotaru, R. Teodorescu, and F. Blaabjerg, "Advanced grid synchronization system for power converters under unbalanced and distorted operating conditions," in *Proc. Annu Conf. IEEE Ind. Electron. Soc.*, Nov. 2006, pp. 5173–5178.

[13] P. Rodriguez, A. Luna, I. Etxeberria, J. Hermoso, and R. Teodorescu, "Multiple second order generalized integrators for harmonic synchronization of power converters," *Proc. IEEE Energy Convers. Congr. Expo.*, pp. 2239–2246, Sep. 2009.

[14] P. Rodriguez, A. Luna, I. Candela, R. Mujal, R. Teodorescu, and F. Blaabjerg, "Multiresonant frequency—locked loop for grid synchronization of power converters under distorted grid conditions," *IEEE Trans. Ind. Electron.*, vol. 58, no. 1, pp. 127–138, Jan. 2011.

[15] E. Robles, S. Ceballos, J. Pou, J. Martín, J. Zaragoza, and P. Ibañez, "Variable—frequency grid—sequence detector based on a quasi—ideal low—pass filter stage and a phase—locked loop," *IEEE Trans. Power Electron.*, vol. 25, no. 10, pp. 2552–2563, Oct. 2010.

[16] E. Robles, J. Pou, S. Ceballos, J. Zaragoza, J. Martín, and P. Ibañez, "Frequency-adaptive stationary-reference-frame grid voltage sequencedetector for distributed generation systems," *IEEE Trans. Ind. Electron.*, vol. 58, no. 9, pp. 4275–4287, Sep. 2011.

[17] G. Xiaoqiang, W. Weiyang, and C. Zhe, "Multiple—complex coefficientfilter—based phase—locked loop and synchronization technique for three—phase grid—interfaced converters in distributed utility networks," *IEEE Trans. Ind. Electron.*, vol. 58, no. 4, pp. 1194–1204, Apr. 2011.

[18] S. G. Jorge, C. Busada, and J. Solsona, "Frequency adaptive discrete filter for grid synchronization under distorted voltages," *IEEE Trans. Power Electron.*, vol. 27, no. 8, pp. 3584–3594, Aug. 2012.

[19] G. Escobar, M. Martinez—Montejano, A. Valdez, P. Martinez, and M. Hernandez—Gomez, "Fixed-reference-frame phase-locked loop for grid synchronization under unbalanced operation," *IEEE Trans. Ind. Electron.*, vol. 58, no. 5, pp. 1943–1951, May 2011.

[20] M. Sun and Z. Sahinoglu, "Extended Kalman filter based grid synchronization in the presence of voltage unbalance for smart grid," *Proc. IEEE PES Innovative Smart Grid Technol.*, pp. 1–4, Jan. 2011.

[21] R. Marino and P. Tomei*, Nonlinear Control Design. Geometric, Adaptive and Robust*. Upper Saddle River, NJ: Prentice-Hall, 1995.

Sebastian Gomez Jorge received the Electronic Engineer degree, the M.S. degree in electrical engineering, and the Dr. degree in engineering from the Universidad Nacional del Sur, Bahía Blanca, Argentina, in 2006, 2009, and 2011, respectively.

Currently, he is with the Departamento de Ingeniería Eléctrica y de Computadoras, Instituto de Investigaciones en Ingeniería Eléctrica "Alfredo C. Desages" (IIIE), Universidad Nacional del Sur, Bahía Blanca, Argentina, where he is a graduate Teaching Assistant, and with CONICET.

Jorge A. Solsona (SM'04) received the Electronics Engineer and Dr. degrees from the Universidad Nacionalde La Plata, La Plata, Argentina, in 1986 and 1995, respectively.

Currently, he is with the Departamento de Ingeniería Eléctrica y de Computadoras, Instituto de Investigaciones en Ingeniería Eléctrica "Alfredo C. Desages" (IIIE), Universidad Nacional del Sur, Bahía Blanca, Argentina, where he is a Professor and with CONICET. He is involved in teaching and research on control theory and its applications in electromechanical systems.

Claudio A. Busada was born in Bahía Blanca, Argentina, on March 13, 1962. He received the degree in electrical engineering and the Dr. degree in control systems from the Universidad Nacional del Sur, Bahía Blanca, Argentina, in 1989 and 2004, respectively.

From 1988 to 2004, he was with the Mechanic and Electrical Department, City of Bahía Blanca. Since 1989, he has been with the Departamento de Ingeniería Eléctrica y de Computadoras (DIEC), Universidad Nacional del Sur, where he is a Professor. He is a Researcher with the Instituto de Investigaciones en Ingeniería Eléctrica "Alfredo C. Desages" (UNS-CONICET). His research interests include power electronics, rotating machinery, active filters, automatic control, and integration of distributed energy systems.